preting the change in reaction time with particle size. Accordingly, an attempt was made to estimate the amount of reaction occurring for each amatol mix in the following way. It was assumed that complete reaction had occurred by the time at which $V = 1.2$ cc/g for the smallest particle size. [This volume was much larger than that at which the peak in $(dP/d\rho)^{\frac{1}{2}}$ occurred for any of the particle sizes.] The area under the PV curve for Mix 0 from $V = 1.2$ cc/g to zero pressure was obtained as the difference between the total energy release and the measured area from the shock to $V = 1.2$ cc/g, less the shock energy $\frac{1}{2}P_1(V_0 - V_1)$. It was then assumed that the isentropic expansion from $V = 1.2$ cc/g followed a constant γ law, for which $E = PV/(\gamma - 1)$ then determined the effective value of γ. The value of γ thus determined for the finest AN particle size was then used to determine the area under the "tails" of all the other PV curves from $V = 1.2$ cc/g to zero pressure. It felt is that this calculation (see Fig. 11) afforded a reasonable, if crude, estimate of the energy release up to $V = 1.2$ cc/g.

Radiographic Experiments

In addition to the optical work, flash radiography was employed, for a twofold purpose, (1) to examine the major assumption made in the work, that of negligible variation of properties on cross-channel lines, and (2) to obtain a crude check on the density profiles obtained in the optical work. The explosive was viewed parallel to the confining plates and was loaded to the same density as in the optical work.

In adapting the one-dimensional channel flow arrangement to allow radiography, the width of the channel was reduced from 8 to 4 in., and the lateral edges were covered with 0.120-in.-thick glass rather than massive steel. The cells were again formed by parallel $\frac{1}{4}$-in.-thick plates of 304 stainless steel. The method of radiography and film protection used has been described previously.[9]

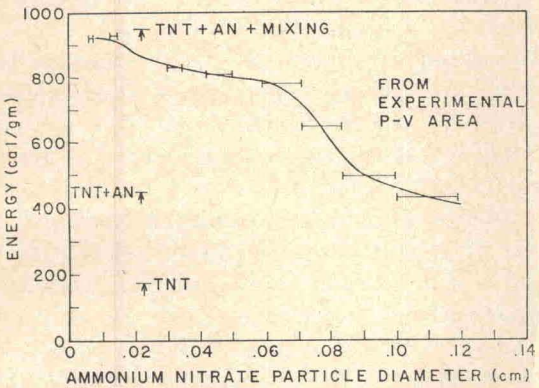

FIG. 11. Energy versus particle diameter of ammonium nitrate. Illustrated are the curves obtained from the experimental P–V data. The total energies to be expected from the various reaction steps are indicated.

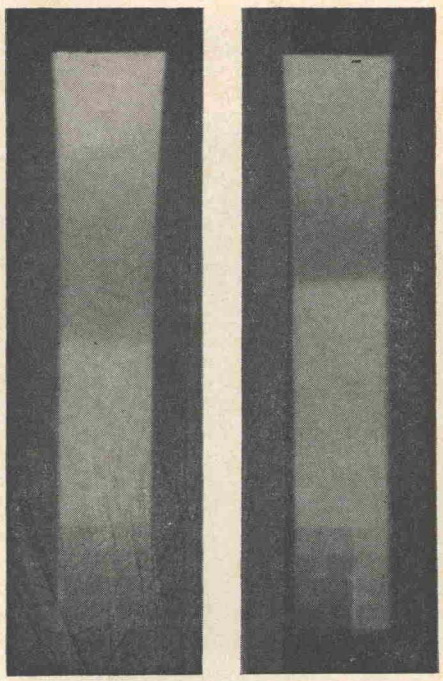

FIG. 12. Radiographs of detonation in one-dimensional channel flow for mixes G (left) and C (right). The aluminum "step wedges" are visible in the lower parts of the radiographs. The detonation is proceeding in both cases from top to bottom. The radiographs illustrate the relatively small expansion of the stream tube with this confinement.

The density of the explosive behind the detonation front was obtained by measuring the optical density of the radiograph with a Jarrel–Ash Model 21-000 Microphotometer at a slit size of 1.5 mm × 15 μ and comparing the readings for the explosive with readings from an aluminum step wedge in the field of view. The aluminum step wedge had been calibrated against a step wedge of the same explosive at the same density with the same x-ray flash voltage (500 kV) used in the detonation shot. Two of the radiographs are shown in Fig. 12. Densitometer readings across the 0.5-in.-wide channel at any fixed distance from the detonation front indicated no detectable density variations on cross-channel lines.

Curvature of the detonation front made it impossible to obtain from the radiograph an unambiguous, density profile downstream from the detonation front. Whereas, in the optical work measurements were made near the center line of the plates where curvature is minimal, the x-ray path extended through the full width of the explosive, including

[9] A. S. Balchan, J. Appl. Phys. 34, 241 (1963).

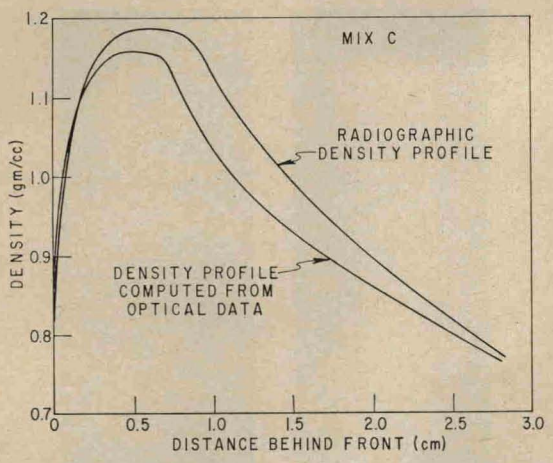

FIG. 13. Comparison of radiographic and "smeared" optical density profiles for Mix *C*.

the edge zones where the curvature is greatest. The reduced width and edge confinement required in the radiographic work further enhanced the curvature effects. A comparison of optical and radiographic results was obtained by computing an apparent density profile in the narrow cells from the optically obtained density profile and the curvature of the front. The curvature in the smaller cells was measured by a modified grid reflection technique with explosive shots identical to the x-ray shots. It was assumed that the optically obtained density profile did not vary along the x-ray path, the whole profile being displaced downstream in accord with the curvature of the front. The apparent density profiles obtained by averaging along the x-ray path were compared with the radiographically observed profiles for four different explosive mixtures. For brevity, one typical comparison is shown in Fig. 13; agreement in the other three experiments was as good as that illustrated.

It was concluded that the radiographic experiments provided adequate justification for the one-dimensional flow assumption and indicated that no gross errors in measurements of flow properties were made in the optical work.

DISCUSSION OF RESULTS

The most obvious feature of the present results is the occurrence of a relatively thin high-pressure zone immediately behind the shock front in all but the coarsest amatol mixes; the zone is most clearly developed where the AN particle size is smallest. The dominance of chemical reaction in the fine-grained mixtures is clearly demonstrated in the P–V curves (Fig. 9), where the pressure drops to about half the peak value along a line which barely deviates from the Rayleigh line. As shown in Fig. 6, in the Zeldovich–von Neumann–Doering model the quantity $(dP/d\rho)^{\frac{1}{2}}$ rises along the velocity (q) curve until it reaches its maximum value at the Chapman–Jouguet point, where the velocity is sonic, and where, in the Zeldovich–von Neumann–Doering model, reaction is complete. In the more fine-grained mixtures, $(dP/d\rho)^{\frac{1}{2}}$ follows the q curve almost to its maximum value and then falls sharply as q continues to rise because of lateral expansion. The location of the maximum $(dP/d\rho)^{\frac{1}{2}}$ must therefore lie close to the Chapman-Jouguet point in the fine-grained explosives.

As the AN particle size is increased, the pressure profile in the reaction zone becomes less steep; and for the coarsest size studied (Mix *G*), the pressure is almost flat. Apparently in the coarse mixtures the rate of energy release behind the front is so low that it barely predominates over lateral expansion. Since the rate of lateral expansion rises steadily from an initial zero value, the rate of chemical energy release must be rather low near the detonation front and probably increases downstream, at a rate which is necessarily slower than the rate of increase of the rate of lateral expansion, since the two effects must be equal at the Chapman–Jouguet point. As pointed out earlier, the pressure can show a rise in the initial part of the reaction zone, but this was not observed in the range of particle sizes studied.

Since the decomposition of the very fine TNT component should be fast, even in the mixtures with coarse AN, it appears likely that the TNT reaction is occurring too fast to be resolved adequately. In the coarse AN mixtures it is quite possible that the TNT reaction is occurring partly in the shock front zone, which must extend over a few particle diameters, i.e., a few millimeters.

The complex variation of effective reaction time τ versus AN particle diameter for fixed explosive thickness ($\frac{1}{2}$ in.) and confinement ($\frac{1}{4}$-in. stainless-steel plates), shown by the heavy curve in Fig. 10, can be accounted for qualitatively on the basis of the three-stage chemical energy release and the effects of greater lateral expansion relative to the extent of reaction and lower detonation velocity as the particle diameter increases. We use as a guide the curve of Fig. 11 which shows the rough estimate of chemical energy release up to the point where the volume was 1.2 cc/g, and we note that the energy release in the effective reaction zone is less than this curve. In the range of small particle